Journal of Computational Physics **176,** 70–92 (2002)
doi:10.1006/jcph.2001.6968, available online at http://www.idealibrary.com on IDEAL®

2D Simulation of a Silicon MESFET with a Nonparabolic Hydrodynamical Model Based on the Maximum Entropy Principle

Vittorio Romano

Dipartimento di Matematica e Informatica, Universitá di Catania, viale A. Doria 6, 95125 Catania, Italy
E-mail: romano@dmi.unict.it, URL: http://www.dmi.unict.it/~romano

Received May 9, 2001; revised November 7, 2001

A hydrodynamical model for electron transport in silicon semiconductors, which is free of any fitting parameters, has been formulated on the basis of the maximum entropy principle. The model considers the energy band to be described by the Kane dispersion relation and includes electron–nonpolar optical phonon and electron–acoustic phonon scattering. The set of balance equations of the model forms a quasilinear hyperbolic system and for its numerical integration a recent high-order shock-capturing central differencing scheme has been employed. Simulations of an n^+–n–n^+ silicon diode have been presented and comparison with Monte Carlo data shows the good accuracy of the model and performance of the numerical scheme. Here the results of simulations of a silicon MESFET in the two-dimensional case are presented. Both the model and the numerical scheme demonstrate their accuracy and efficiency as CAD tools for modeling realistic submicron electron devices. © 2002 Elsevier Science (USA)

Key Words: charge transport; hydrodynamical models; numerical methods for hyperbolic systems; electron devices.

1. INTRODUCTION

Modeling modern submicron electron devices requires an accurate description of charge transport in order to cope with high-field phenomena that cannot be described satisfactorily within the framework of the *drift–diffusion equations* [10–12] since these do not include energy as a dynamical variable and are valid only in the quasi-stationary limit. Generalizations of the drift–diffusion equations have been sought which do not suffer from these shortcomings. These models are loosely termed *hydrodynamical models*, this class comprising also the so-called *energy models* [13–15]. Hydrodynamical models are obtained from the infinite hierarchy of the moment equations of the Boltzmann transport equation

0021-9991/02 $35.00
© 2002 Elsevier Science (USA)
All rights reserved.

using a suitable truncation procedure. However, most hydrodynamical models suffer from serious theoretical drawbacks due to the ad hoc treatment of the closure problem [19]. Recently in [1, 2] a moment approach has been introduced in which the closure procedure is based on the maximum entropy principle, while the energy bands are described by the Kane dispersion relation. The resulting model, which can be cast in the framework of extended thermodynamics [16, 17] or equivalently of Levermore's moment theory [18], comprises balance equations of electron density, energy density, velocity, and energy flux, coupled to the Poisson equation for the electric potential. The presence of a balance equation for energy flux is at variance with the standard hydrodynamical models usually employed, which are based on Navier–Stokes–Fourier like equations [20, 21]. Moreover, apart from the Poisson equation, the system is hyperbolic in the physically relevant region of the field variables.

A numerical scheme for problems of this kind based on central differencing has been developed in [5, 6, 22] for the one-dimensional case and applied in [7, 9] to bulk silicon and to an n^+–n–n^+ silicon diode (for the parabolic band case see [23]). The obtained results are rather encouraging regarding the accuracy of the model and the performance of the numerical scheme. Here we investigate further the capability of the model by extending the numerical scheme to the bidimensional case and simulating a silicon MESFET.

2. THE MODEL

Here we give only a brief sketch of the model. For more details the interested reader is referred to [1, 2].

In the model one assumes that the conduction band [27] is described around each minimum (valley) by the Kane dispersion relation approximation

$$\mathcal{E}(k)[1+\alpha\mathcal{E}(k)] = \frac{\hbar^2 k^2}{2m^*}, \quad \mathbf{k} \in \mathcal{R}^3, \tag{1}$$

where $\mathcal{E}$ is the electron energy, α is the nonparabolicity parameter, m^* is the effective electron mass, $\hbar\mathbf{k}$ is the *crystal momentum*, which is assumed to vary in all the space $\mathcal{R}^3$, and $\hbar$ is the Planck constant h divided by 2π. The values of α and the other physical parameters are reported in Table 1 in the Appendix. Concerning the collision term, the most relevant interactions for silicon, that is, those between electrons and nonpolar optical phonons and acoustic phonons, have been taken into account. Electron–electron scattering and scattering of electrons with ionized impurities are not considered here.

The macroscopic balance equations are deduced by taking the moments of the Boltzmann transport equation for electrons in semiconductors [12]; that is, by multiplying the transport equation by weight functions $\psi(\mathbf{k})$ and integrating over $\mathcal{R}^3$. If we consider the set of weight functions 1, $\hbar\mathbf{k}$, $\mathcal{E}$, and $\mathcal{E}\,\mathbf{v}$, we get the following macroscopic balance equations:

$$\frac{\partial n}{\partial t} + \frac{\partial(nV^i)}{\partial x^i} = 0, \tag{2}$$

$$\frac{\partial(nP^i)}{\partial t} + \frac{\partial(nU^{ij})}{\partial x^j} + neE^i = nC_P^i, \tag{3}$$

$$\frac{\partial(nW)}{\partial t} + \frac{\partial(nS^j)}{\partial x^j} + neV_k E^k = nC_W, \tag{4}$$

$$\frac{\partial(nS^i)}{\partial t} + \frac{\partial(nF^{ij})}{\partial x^j} + neE_j G^{ij} = nC_W^i. \tag{5}$$

This system is coupled to Poisson's equation,

$$\mathbf{E} = -\nabla\Phi, \quad \epsilon\Delta\Phi = -e(n_D - n_A - n), \tag{6}$$

where $\mathbf{E}$ represents the self-consistent electric field, Φ is the electric potential, e is the elementary charge, n_D and n_A are the donor and acceptor densities, respectively, ϵ is the dielectric constant, and n is the particle density. We consider the unipolar case and therefore the hole concentration is not included.

The macroscopic quantities involved in the balance equations are related to the one-particle distribution function of electrons $f(\mathbf{x}, t, \mathbf{k})$ as follows,

$$n = \int_{\mathcal{R}^3} f\, d^3\mathbf{k} \text{ is the electron density,} \tag{7}$$

$$V^i = \frac{1}{n}\int_{\mathcal{R}^3} f v^i\, d^3\mathbf{k} \text{ is the average electron velocity,} \tag{8}$$

$$W = \frac{1}{n}\int_{\mathcal{R}^3} \mathcal{E}(k) f\, d^3\mathbf{k} \text{ is the average electron energy,} \tag{9}$$

$$S^i = \frac{1}{n}\int_{\mathcal{R}^3} f v^i \mathcal{E}(k)\, d^3\mathbf{k} \text{ is the energy flux,} \tag{10}$$

$$P^i = \frac{1}{n}\int_{\mathcal{R}^3} f\hbar k^i\, d^3\mathbf{k} = m^*(V^i + 2\alpha S^i) \text{ is the average crystal momentum,} \tag{11}$$

$$U^{ij} = \frac{1}{n}\int_{\mathcal{R}^3} f v^i \hbar k^j\, d^3\mathbf{k} \text{ is the flux of crystal momentum,} \tag{12}$$

$$G^{ij} = \frac{1}{n}\int_{\mathcal{R}^3} \frac{1}{\hbar} f \frac{\partial}{\partial k_j}(\mathcal{E} v_i)\, d^3\mathbf{k}, \tag{13}$$

$$F^{ij} = \frac{1}{n}\int_{\mathcal{R}^3} f v^i v^j \mathcal{E}(k)\, d^3\mathbf{k} \text{ is the flux of energy flux,} \tag{14}$$

$$C_P^i = \frac{1}{n}\int_{\mathcal{R}^3} \mathcal{C}[f]\hbar k^i\, d^3\mathbf{k} \text{ is the production of the crystal momentum balance equation,} \tag{15}$$

$$C_W = \frac{1}{n}\int_{\mathcal{R}^3} \mathcal{C}[f]\mathcal{E}(k)\, d^3\mathbf{k} \text{ is the production of the energy balance equation,} \tag{16}$$

$$C_W^i = \frac{1}{n}\int_{\mathcal{R}^3} \mathcal{C}[f] v^i \mathcal{E}(k)\, d^3\mathbf{k} \text{ is the production of the energy flux balance equation,} \tag{17}$$

where $\mathcal{C}[f]$ is the scattering term in the electron transport equation.

These moment equations do not constitute a set of closed relations because of the fluxes and production terms. Therefore constitutive assumptions must be prescribed.

If we assume as fundamental variables n, V^i, W, and S^i, which have a direct physical interpretation, the closure problem consists of expressing P^i, U^{ij}, F^{ij}, and G^{ij} and the moments of the collision term C_P^i, C_W, and C_W^i as functions of n, V^i, W, and S^i.

The maximum entropy principle (hereafter MEP) leads to a systematic way of obtaining constitutive relations on the basis of information theory. According to the MEP, if some moments M_A are known, the distribution function f_{ME} which can be used to evaluate the unknown moments of f corresponds to the extremum of the entropy functional under the constraint that it yields exactly the known moments M_A; that is,

$$\int_{\mathcal{R}^3} \psi_A f_{ME}\, d^3\mathbf{k} = M_A, \tag{18}$$

with $\psi_A(\mathbf{k})$ the weight function entering into the definition of the moments M_A. Once the expression for f_{ME} has been obtained, one gets the closure relations by evaluating the expressions (7)–(17) with $f = f_{ME}$.

This procedure, which fits into the framework of extended thermodynamics [16, 17] or equivalently Levermore's moment theory [18], has been used in [1, 2] upon the ansatz of small anisotropy for f_{ME} since Monte Carlo simulations for electron transport in Si show that the anisotropy of f is small even far from equilibrium.

Formally a *small* anisotropy parameter δ was introduced and explicit constitutive equations were obtained for high-order fluxes [1] and for the production terms up to second order in δ [2]. However, it was found in [7] that the first-order model is sufficiently accurate for numerical applications and avoids some irregularities due to nonlinearities, as in the parabolic band case [23]. A similar approach was followed in [24, 25], where the smallness of the anisotropy was used to justify the truncation of the expansion of the distribution function in spherical harmonics up to the harmonics of order zero and one.

Up to first order the constitutive equations for fluxes are of the form

$$U_{ij} = U(W)\delta_{ij}, \quad F_{ij} = F(W)\delta_{ij}, \quad G_{ij} = G(W)\delta_{ij}. \tag{19}$$

The explicit expressions of $U(W)$, $F(W)$, and $G(W)$ are given in [1, 2] and are reported in the Appendix. Note that they depend only on W. In the parabolic band approximation ($\alpha = 0$) one finds

$$U_{ij}^P = \frac{2}{3}W\delta_{ij}, \quad m^* F_{ij}^P = \frac{10}{9}W^2\delta_{ij}, \quad m^* G_{ij} = \frac{5}{3}W\delta_{ij}. \tag{20}$$

We remark that in [1], instead of the variable S_i, the vector $N_i = \int_{\mathcal{R}^3} f\hbar k^i \mathcal{E}(k)\, d^3\mathbf{k}$ was introduced and therefore a different moment equation (5) was considered. The choice of N_i was made by following [26] with the aim of comparing the MEP closure relations with those reported in [26], obtained by the analysis of Monte Carlo data. Both the choice are theoretically valid. However, in the simulations, the use of S_i is more practical for time-dependent simulations because one avoids the presence of a constitutive equation in the vector of the conserved variable (see Section 3). Moreover S_i has a direct physical meaning.

The production term of the energy can be put in the form

$$C_W = -\frac{W - W_0}{\tau_W(W)}, \tag{21}$$

where $\tau_W(W)$ is the energy relaxation time. The expression of C_W is given in the Appendix. The term W_0 represents the equilibrium energy $\frac{3}{2}k_B T_L$, with T_L the lattice temperature.

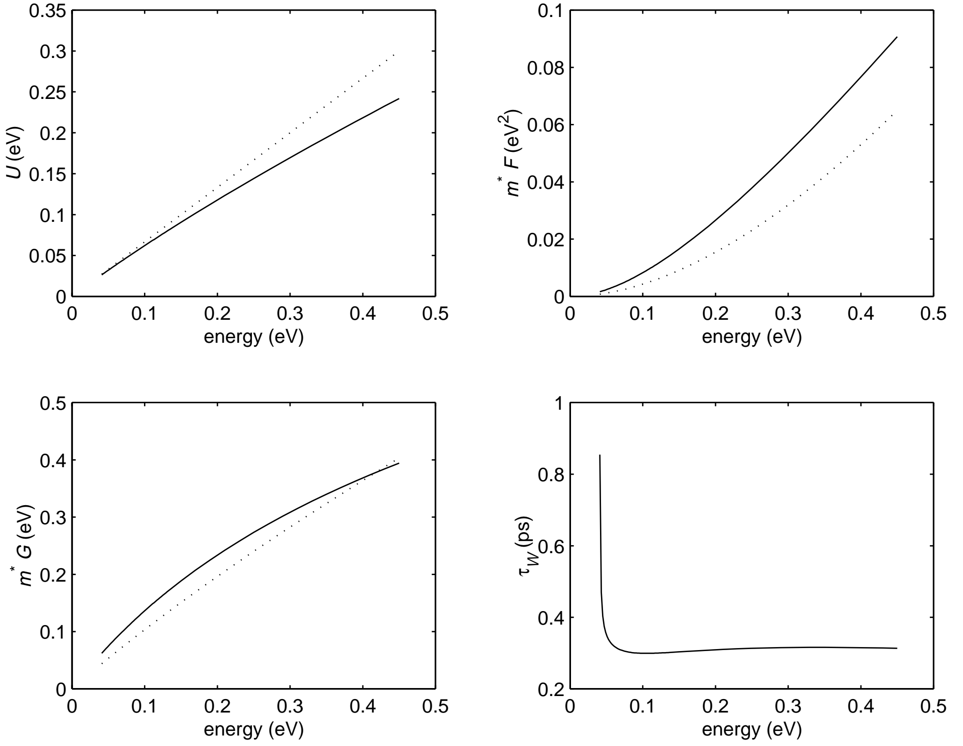

FIG. 1. Fluxes U, F, G, and energy relation time τ_W versus energy W (eV) for the Kane dispersion relation. For comparison we have also plotted U, F, G in the case of the parabolic band approximation (dotted line) (see Eqs. (20)).

The production terms of crystal momentum and energy flux can be written as

$$C_P^i = c_{11}(W)V_i + c_{12}(W)S_i, \tag{22}$$

$$C_W^i = c_{21}(W)V_i + c_{22}(W)S_i. \tag{23}$$

(For the expressions of the coefficients $c_{ij}(W)$ see the Appendix.)

In Fig. 1 we plot U, F, G, and τ_W versus energy and in Fig. 2 we plot c_{11}, c_{12}, c_{21}, and c_{22} versus energy in the case of Kane's dispersion relation and in the parabolic approximation.

In the two-dimensional case the complete system of equations can be put into the equivalent form, where Eq. (3) has been replaced with a linear combination with Eq. (5) by taking into account the relation (11)

$$\frac{\partial}{\partial t}F^{(0)}(\mathbf{U}) + \frac{\partial}{\partial x}F^{(1)}(\mathbf{U}) + \frac{\partial}{\partial y}F^{(2)}(\mathbf{U}) = B(\mathbf{U}, \mathbf{E}), \tag{24}$$

$$E_x = -\frac{\partial \Phi}{\partial x}, \quad E_y = -\frac{\partial \Phi}{\partial y}, \tag{25}$$

$$\epsilon\left(\frac{\partial^2 \Phi}{\partial x^2} + \frac{\partial^2 \Phi}{\partial y^2}\right) = e(n - n_D + n_A), \tag{26}$$

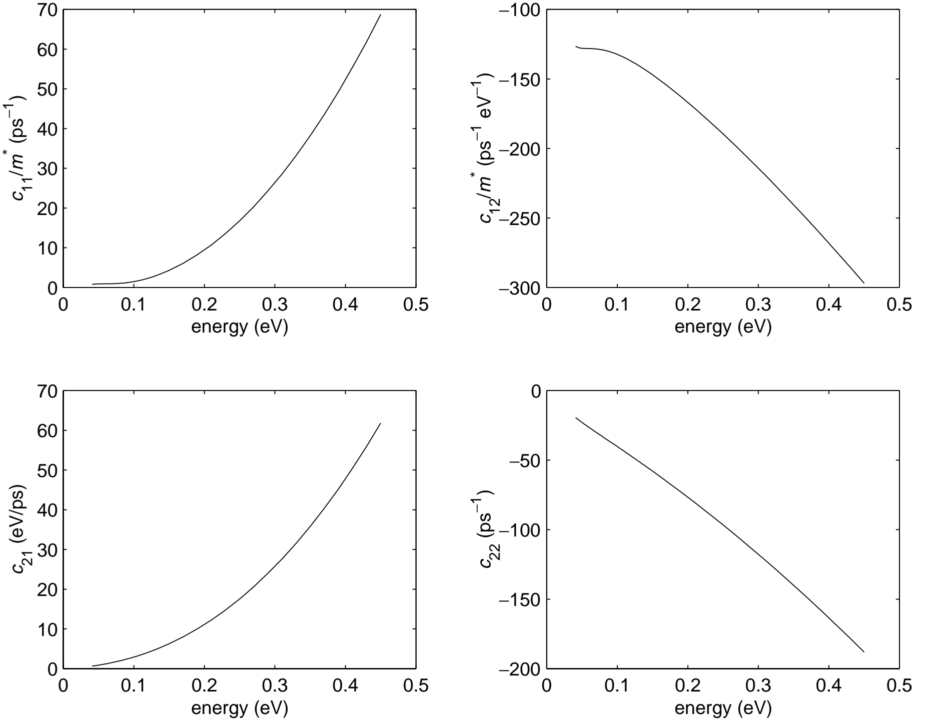

FIG. 2. Coefficients c_{ij} versus energy W (eV) for the Kane dispersion relation.

where

$$\mathbf{U} = \begin{pmatrix} n \\ V^1 \\ V^2 \\ W \\ S^1 \\ S^2 \end{pmatrix}, \quad F^{(0)} = n \begin{pmatrix} 1 \\ m^* V^1 \\ m^* V^2 \\ W \\ S^1 \\ S^2 \end{pmatrix}, \quad F^{(1)} = n \begin{pmatrix} V^1 \\ (U - 2\alpha m^* F) \\ 0 \\ S^1 \\ nF \\ 0 \end{pmatrix},$$

$$F^{(2)} = n \begin{pmatrix} V^2 \\ 0 \\ (U - 2\alpha m^* F) \\ S^2 \\ 0 \\ nF \end{pmatrix},$$

$$B = n \begin{pmatrix} 0 \\ -eE^1(1 - 2\alpha m^* G) + (c_{11} - 2\alpha m^* c_{21})V^1 + (c_{12} - 2\alpha m^* c_{22})S^1 \\ -eE^2(1 - 2\alpha m^* G) + (c_{11} - 2\alpha m^* c_{21})V^2 + (c_{12} - 2\alpha m^* c_{22})S^2 \\ -e\sum_{k=1}^{2} V^k E^k - \frac{W - W_0}{\tau_W} \\ -eE^1 G + c_{21} V^1 + c_{22} S^1 \\ -eE^2 G + c_{21} V^2 + c_{22} S^2 \end{pmatrix}.$$

As proved in [7], the system (24) is hyperbolic in the region $n > 0$, $W \geq W_0$.

3. NUMERICAL METHOD

Numerical integration of quasi-linear hyperbolic systems represents by itself an active research area (see [28, 29]). It is well known that the solutions of quasi-linear systems suffer loss of regularity (e.g., formation of shocks). In the past decades several accurate high-order shock capturing schemes have been developed. Most schemes are based on upwind methods and require the solution to the Riemann problem. Unfortunately no analytical solution to the Riemann problem for the model under investigation is available at the present time and an approach based on the full numerical evaluation of the Roe matrix is not practical. Therefore we have to resort to a central differencing scheme. The central schemes known in the literature deal almost exclusively with homogeneous systems. In [5, 6] a suitable extension for one-dimensional balance laws with (possibly *stiff*) source terms has been developed on the basis of the Nessyahu and Tadmor scheme [3] for homogeneous hyperbolic system. It has been applied in [22, 23] to parabolic band hydrodynamical models of semiconductors. Here we extend the scheme to the bidimensional case starting from the bidimensional version of the Jiang and Tadmor scheme [4].

The complete method is based on a second-order splitting technique. This solves separately the system with the source put equal to zero (convection step) and the flux put equal to zero (relaxation step).

Each convective step has the form of a predictor–corrector scheme [4] on a staggered grid. The scheme is second-order accurate in both time and space for homogeneous systems. If we introduce a uniform grid (x_i, y_j), with $x_{i+1} - x_i = \Delta x =$ constant and $y_{i+1} - y_i = \Delta y =$ constant, and denote by $\Delta t = t^{n+1} - t^n$ the time step, then the convective part of the scheme reads

$$\mathbf{U}_{i,j}^{n+1/2} = \mathbf{U}_{i,j}^{n} - \frac{\lambda}{2} F_{x_{i,j}}^{(1)'} - \frac{\mu}{2} F_{y_{i,j}}^{(2)'}, \tag{27}$$

$$\begin{aligned}
\mathbf{U}_{i+1/2,j+1/2}^{n+1} = {} & \frac{1}{4}\left(\mathbf{U}_{i,j}^{n} + \mathbf{U}_{i,j+1}^{n} + \mathbf{U}_{i+1,j}^{n} + \mathbf{U}_{i+1,j+1}^{n}\right) \\
& + \frac{1}{16}\left(\mathbf{U}'_{x_{i,j}} - \mathbf{U}'_{x_{i+1,j}}\right) - \frac{\lambda}{2}\left[F^{(1)}\left(\mathbf{U}_{i+1,j}^{n+1/2}\right) - F^{(1)}\left(\mathbf{U}_{i,j}^{n+1/2}\right)\right] \\
& + \frac{1}{16}\left(\mathbf{U}'_{x_{i,j+1}} - \mathbf{U}'_{x_{i+1,j+1}}\right) - \frac{\lambda}{2}\left[F^{(1)}\left(\mathbf{U}_{i+1,j+1}^{n+1/2}\right) - F^{(1)}\left(\mathbf{U}_{i,j+1}^{n+1/2}\right)\right] \\
& + \frac{1}{16}\left(\mathbf{U}'_{y_{i,j}} - \mathbf{U}'_{y_{i,j+1}}\right) - \frac{\mu}{2}\left[F^{(2)}\left(\mathbf{U}_{i,j+1}^{n+1/2}\right) - F^{(2)}\left(\mathbf{U}_{i,j}^{n+1/2}\right)\right] \\
& + \frac{1}{16}\left(\mathbf{U}'_{y_{i+1,j}} - \mathbf{U}'_{y_{i+1,j+1}}\right) - \frac{\mu}{2}\left[F^{(2)}\left(\mathbf{U}_{i+1,j+1}^{n+1/2}\right) - F^{(2)}\left(\mathbf{U}_{i+1,j}^{n+1/2}\right)\right],
\end{aligned} \tag{28}$$

where $\lambda = \Delta t/\Delta x$ and $\mu = \Delta t/\Delta y$ denote the fixed-mesh ratios. The time step Δt must satisfy a suitable stability condition (see [4]) that ensures that the generalized Riemann problems with piecewise smooth data at time t^n will not interfere during the time step Δt.

In order to couple the convection step with the relaxation step, it is convenient to make two convection steps of step size $\Delta t/2$, so that the solution is computed on the same grid. A complete convection step is obtained as a sequence of two intermediate steps of time step size $\Delta t/2$.

The values of $\mathbf{U}'_{x_{i,j}}/\Delta x$ and $F'_{x_{i,j}}/\Delta x$ are first-order approximations of the partial derivatives of the field and of the flux with respect to x. They are computed from cell averages by

using a uniform nonoscillatory reconstruction [30],

$$\mathbf{U}'_{x_{i,j}} = \mathrm{MM}\left(d_{x_{i-\frac{1}{2},j}}\mathbf{U} + \frac{1}{2}\mathrm{MM}\left(D_{x_{i-1,j}}\mathbf{U}, D_{x_{i,j}}\mathbf{U}\right), d_{x_{i+\frac{1}{2},j}}\mathbf{U} - \frac{1}{2}\mathrm{MM}\left(D_{x_{i,j}}\mathbf{U}, D_{x_{i+1,j}}\mathbf{U}\right)\right), \tag{29}$$

where

$$D_{x_{i,j}}\mathbf{U} = \mathbf{U}_{i+1,j} - 2\mathbf{U}_{i,j} + \mathbf{U}_{i-1,j},$$
$$d_{x_{i+1/2,j}}\mathbf{U} = \mathbf{U}_{i+1,j} - \mathbf{U}_{i,j}$$

and

$$\mathrm{MM}(x, y) = \begin{cases} \mathrm{sign}(x)\cdot\min(|x|, |y|) & \text{if } \mathrm{sign}(x) = \mathrm{sign}(y) \\ 0 & \text{otherwise.} \end{cases}$$

A similar procedure is used for evaluating $F^{(1)}_{x_{i,j}}$. The computation of $\mathbf{U}'_{y_{i,j}}/\Delta y$ and $F^{(2)}_{y_{i,j}}/\Delta y$ proceeds along similar lines.

The electric potential is calculated from the Poisson equation (26) with a standard procedure based on central differencing and by resorting to the conjugate gradient method to solve the resulting linear system.

In the relaxation step one has to solve the following system of ordinary differential equations (ODEs):

$$\begin{aligned}
\frac{dn}{dt} &= 0, \\
\frac{dV_k}{dt} &= -\frac{eE_k}{m^*} + 2\alpha e E_k G + \left(\frac{c_{11}}{m^*} - 2\alpha c_{21}\right)V_k + \left(\frac{c_{12}}{m^*} - 2\alpha c_{22}\right)S_k, \quad k = 1, 2, \\
\frac{dW}{dt} &= -e\sum_{p=1}^{2} V_p\, E_p - \frac{W - W_0}{\tau_W}, \\
\frac{dS_k}{dt} &= -eE_k G + c_{21}V_k + c_{22}S_k, \quad k = 1, 2.
\end{aligned}$$

By freezing the energy relaxation time, the coefficients c_{lp} and $G(W)$, and the electric field at $t = t^n$, we can discretize these equations for each grid point (x_i, y_j) in a semiimplicit way as

$$\begin{aligned}
\frac{n^{n+1}_{i,j} - n^n_{i,j}}{\Delta t} &= 0, \\
\frac{V^{n+1}_{k_{i,j}} - V^n_{k_{i,j}}}{\Delta t} &= -\frac{eE^n_k}{m^*} + 2\alpha e E^n_k G^n + \left(\frac{c^n_{11}}{m^*} - 2\alpha c^n_{21}\right)V^{n+1}_{k_{i,j}} \\
&\quad + \left(\frac{c^n_{12}}{m^*} - 2\alpha c^n_{22}\right)S^{n+1}_{k_{i,j}}, \quad k = 1, 2, \\
\frac{W^{n+1}_{i,j} - W^n_{i,j}}{\Delta t} &= -e\sum_{p=1}^{2} V^n_p\, E^n_p - \frac{W^{n+1}_{i,j} - W_{0_{i,j}}}{\tau^n_W},
\end{aligned}$$

$$\frac{S^{n+1}_{k_{i,j}} - S^n_{k_{i,j}}}{\Delta t} = -eE^n_k G^n + c^n_{21} V^{n+1}_{k_{i,j}} + c^n_{22} S^{n+1}_{k_{i,j}}, \quad k = 1, 2,$$

which gives

$$n^{n+1}_{i,j} = n^n_{i,j}, \tag{30}$$

$$V^{n+1}_{k_{i,j}} = \frac{1}{\delta^n}\left[\left(1 - c^n_{22}\Delta t\right) d^n_{1_k} + d^n_{2_k}\Delta t\left(\frac{c^n_{12}}{m^*} - 2\alpha c^n_{22}\right)\right], \quad k = 1, 2, \tag{31}$$

$$W^{n+1}_{i,j} = \left(1 + \frac{\Delta t}{\tau^n_W}\right)^{-1}\left[W^n_{i,j} + \left(-e\sum_{p=1}^{2} E^n_p V^n_p + \frac{W_{0_{i,j}}}{\tau^n_W}\right)\Delta t\right], \tag{32}$$

$$S^n_{k_{i,j}} = \frac{1}{\delta^n}\left\{c^n_{21} d^n_{1_k}\Delta t + d^n_{2_k}\left[1 - \left(\frac{c^n_{11}}{m^*} - 2\alpha c^n_{21}\right)\Delta t\right]\right\}, \quad k = 1, 2, \tag{33}$$

where

$$\delta^n = (1 - c_{22}\Delta t)\left[1 - \left(\frac{c^n_{11}}{m^*} - 2\alpha c^n_{21}\right)\Delta t\right] - c_{21}\left(\frac{c^n_{12}}{m^*} - 2\alpha c^n_{22}\right)(\Delta t)^2,$$

$$d^n_{1_k} = V^n_k + \left(-\frac{eE^n_k}{m^*} + 2\alpha e E^n_k G^n\right)\Delta t, \quad k = 1, 2,$$

$$d^n_{2_k} = S^n_k - eE^n_k G^n \Delta t, \quad k = 1, 2.$$

The simple splitting outlined above is only first-order accurate. In order to get a full second-order scheme we combine the relaxation and convective steps in the same way as proposed in [5, 6] for the one-dimensional case. Note that the analysis of the splitting accuracy does not really depend on the dimension of the space. Given the fields U^n and E^n at time t^n, the fields at time t^{n+1} are obtained using

$$\begin{aligned}
\mathbf{U}_1 &= \mathcal{R}(\mathbf{U}^n, \mathbf{E}^n, \Delta t),\\
\mathbf{U}_2 &= \frac{3}{2}\mathbf{U}^n - \frac{1}{2}\mathbf{U}_1,\\
\mathbf{U}_3 &= \mathcal{R}(\mathbf{U}_2, \mathbf{E}^n, \Delta t),\\
\mathbf{U}_4 &= \mathcal{C}(\mathbf{U}_3, \Delta t),\\
\mathbf{E}^{n+1} &= \mathcal{P}(\mathbf{U}_4),\\
\mathbf{U}^{n+1} &= \mathcal{R}(\mathbf{U}_4, \mathbf{E}^{n+1}, \Delta t/2),
\end{aligned}$$

where $\mathcal{R}(\mathbf{V}, \mathbf{E}, \Delta t)$ represents the discrete operator corresponding to the implicit relaxation step (30)–(33) with initial condition $\mathbf{V}$, constant in time electric field $\mathbf{E}$, and time step Δt; $\mathcal{C}(\mathbf{V}, \Delta t)$ is the discrete operator corresponding to the convective scheme (27)–(29) with time step Δt and initial condition $\mathbf{V}$; and $\mathcal{P}(U)$ gives the numerical solution to Poisson's equation.

4. SIMULATION OF A SILICON MESFET

In this section we check the validity of our hydrodynamical model and the efficiency of the numerical method by simulating a bidimensional metal semiconductor field effect transistor (MESFET). The shape of the device is taken as rectangular and it is pictured in Fig. 3.

The axes of the reference frame are chosen parallel to the edges of the device. We take the dimensions of the MESFET to be such that the numerical domain is

$$\Omega = [0, 0.6] \times [0, 0.2],$$

where the unit length is the micron.

The regions of high-doping n^+ are the subset

$$[0, 0.1] \times [0.15, 0.2] \cup [0.5, 0.6] \times [0.15, 0.2].$$

The contacts at the source and drain are 0.1 μm wide and the contact at the gate is 0.2 μm wide. The distance between the gate and the other two contacts is 0.1 μm. A uniform grid of 96 points in the x direction and 32 points in the y direction is used. The same doping concentration as used in [31–33] is considered,

$$n_D(x) - n_A(x) = \begin{cases} 3 \times 10^{17}\ \text{cm}^{-3} & \text{in the } n^+ \text{ regions} \\ 10^{17}\ \text{cm}^{-3} & \text{in the } n \text{ region,} \end{cases}$$

with abrupt junctions.

We denote by Γ_D that part of $\partial\Omega$, the boundary of Ω, which represents the source, gate, and drain:

$$\Gamma_D = \{(x, y) : y = 0.2,\ 0 \le x \le 0.1,\ 0.2 \le x \le 0.4,\ 0.5 \le x \le 0.6\}.$$

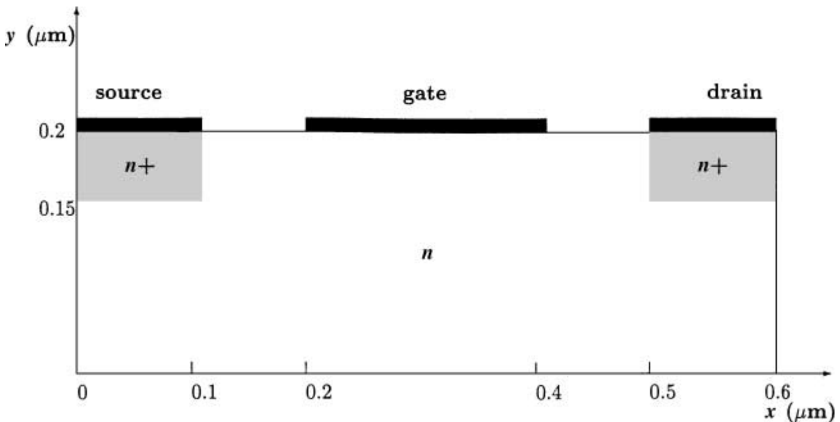

FIG. 3. Schematic representation of a bidimensional MESFET.

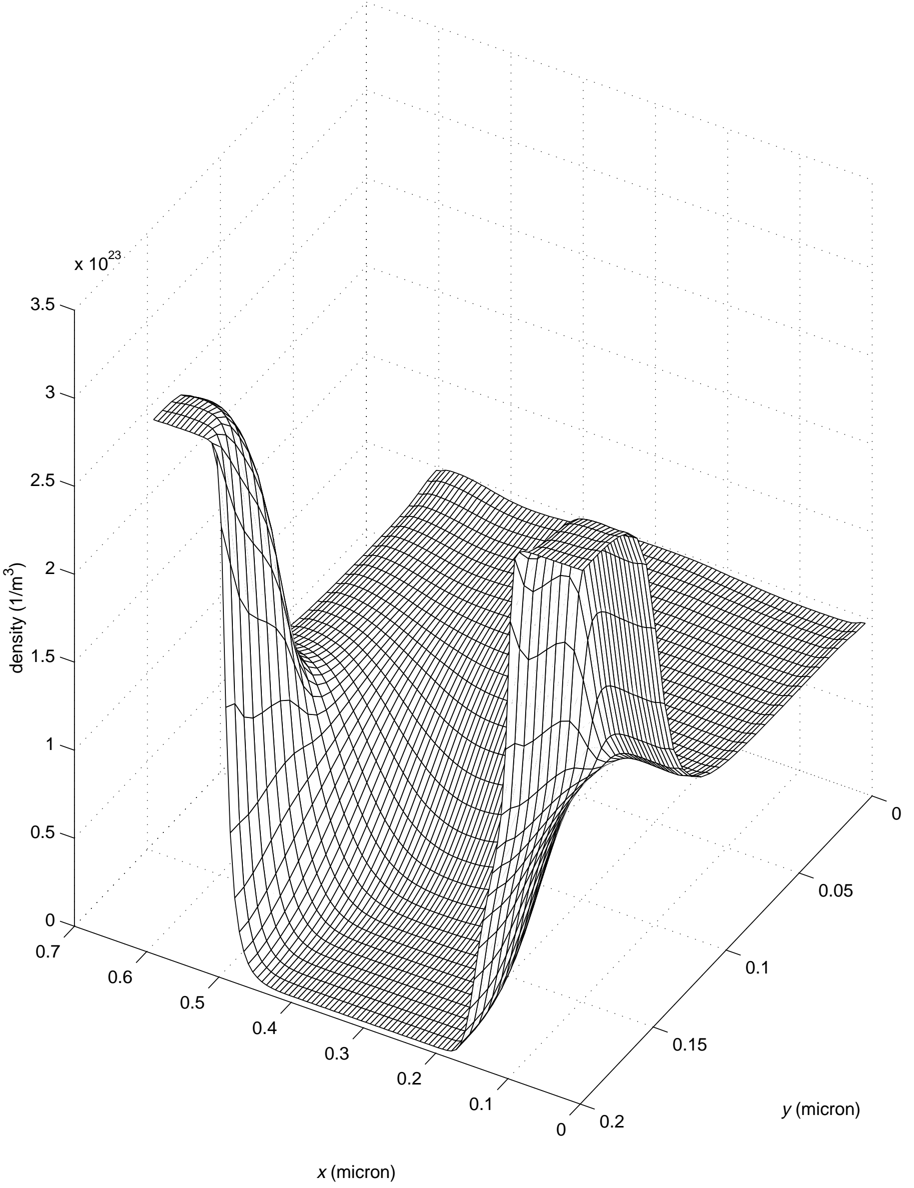

FIG. 4. Stationary solution (after 5 ps) for the density for $\Phi_b = 1$ V.

The other part of $\partial\Omega$ is labeled Γ_N. The boundary conditions are assigned as follows:

$$n = \begin{cases} n^+ & \text{at source and drain} \\ n_g & \text{at gate,} \end{cases} \tag{34}$$

$$\Phi = \begin{cases} 0 & \text{at the source} \\ \Phi_g & \text{at the gate} \\ \Phi_b & \text{at the drain,} \end{cases} \tag{35}$$

$$\begin{cases} W = W_0, & \mathbf{V} \cdot \mathbf{t} = 0, \\ \mathbf{n} \cdot \nabla(\mathbf{V} \cdot \mathbf{n}) = 0, & \mathbf{S} = \frac{5}{3} W_0 \mathbf{V}, \end{cases} \quad \text{on } \Gamma_D, \tag{36}$$

$$\begin{cases} \mathbf{n} \cdot \nabla n = 0, & \mathbf{n} \cdot \nabla W = 0, \quad \mathbf{n} \cdot \nabla \Phi = 0, \\ \mathbf{n} \cdot \nabla V^i = 0, & \mathbf{S} = \frac{5}{3} W \mathbf{V}, \end{cases} \quad i = 1, 2 \quad \text{on } \Gamma_N. \tag{37}$$

Here ∇ is the bidimensional gradient operator while $\mathbf{n}$ and $\mathbf{t}$ are the unit outward normal vector and the unit tangent vector to $\partial\Omega$, respectively. n^+ is the doping concentration in the

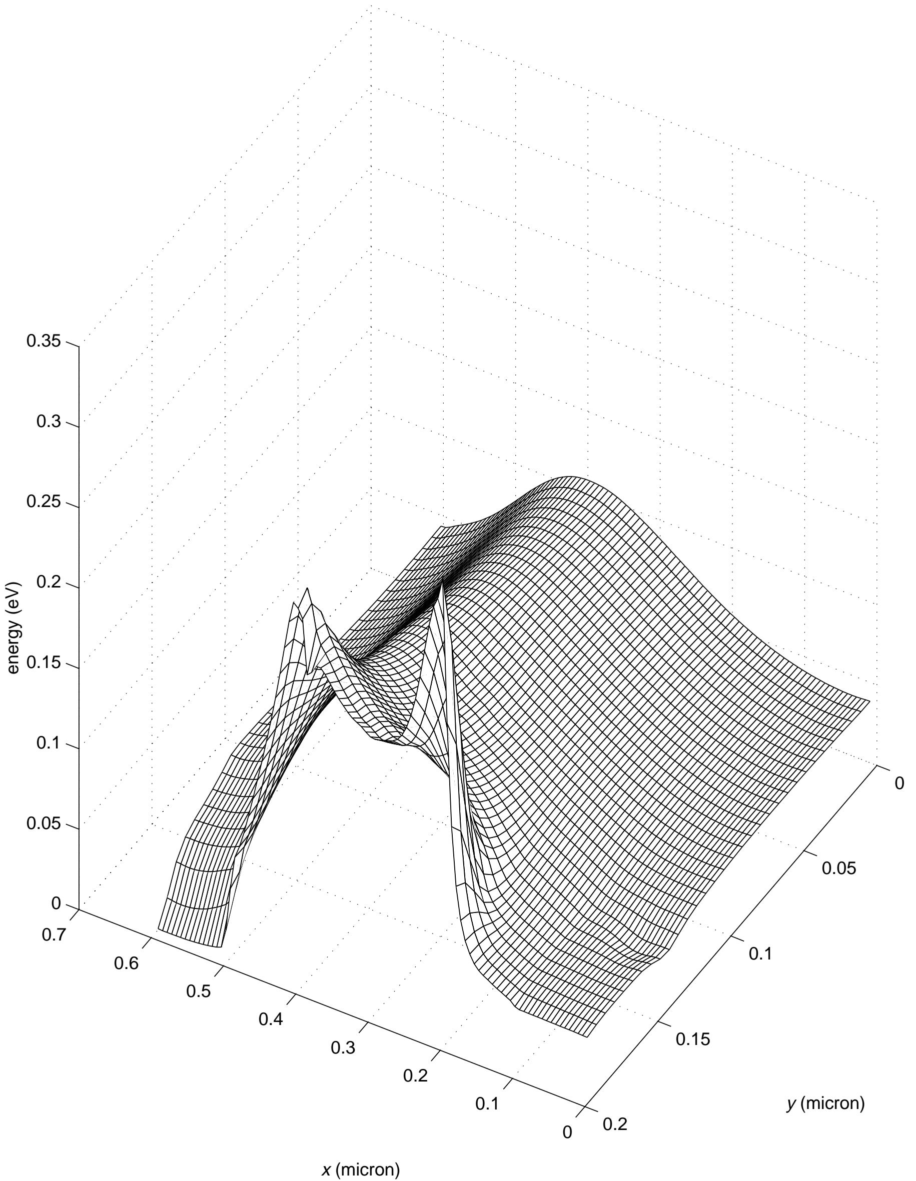

FIG. 5. Stationary solution (after 5 ps) for the energy density for $\Phi_b = 1$ V.

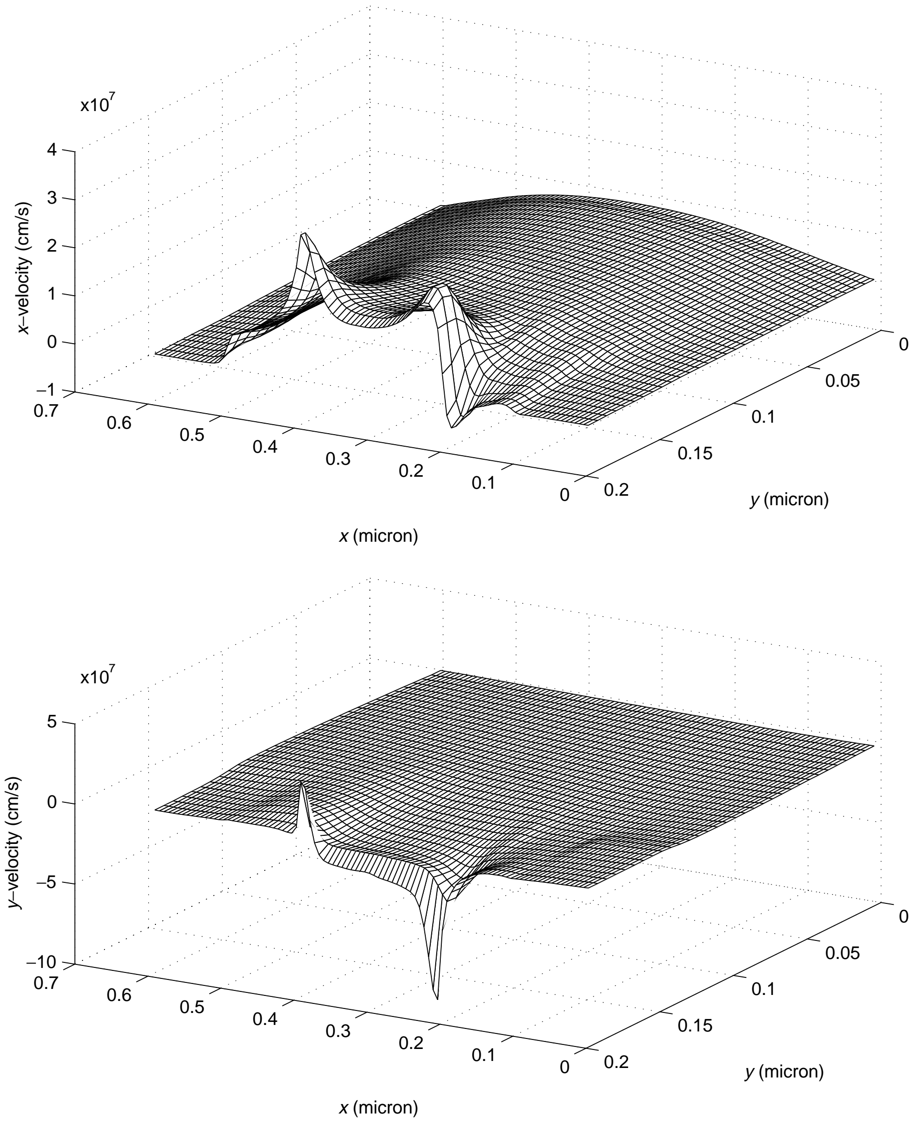

FIG. 6. Stationary solution (after 5 ps) for the x-component and y-component of the velocity for $\Phi_b = 1$ V.

n^+ region and n_g is the density at the gate, which is considered to be a Schottky contact [10]:

$$n_g = 3.9 \times 10^5 \text{ cm}^{-3}.$$

Φ_b is the bias voltage and Φ_g is the gate voltage. In all the simulations we set $\Phi_g = -0.8$ while Φ_b varies.

In the standard hydrodynamical model considered in the literature (e.g., [20. 21]), the energy flux **S** is not a field variable and it is not necessary to prescribe boundary conditions for it. The relations $(36)_4$ and $(37)_5$ are not based on the microscopic boundary conditions for the distribution function, but they may be justified in a heuristic way with the same approach that was followed in [35].

As in [35] we assume that along any interface or surface of a device, the projection of the total energy flux onto the unit normal is a continuous function. In order to have a direct physical meaning of the results, it is better to consider the expression of **S** in the parabolic approximation (see [1]),

$$\mathbf{S} = \frac{5}{2} k_B T \mathbf{V} + \mathbf{q}, \tag{38}$$

where T is the electron temperature defined by $W = \frac{3}{2} k_B T$ and $\mathbf{q}$ is the heat flux. In the previous expression the second-order terms were neglected. By assuming for $\mathbf{q}$ a Fourier-like form $\mathbf{q} = -\kappa \nabla T$, if one does not take into account the contribution of the thermoelectric

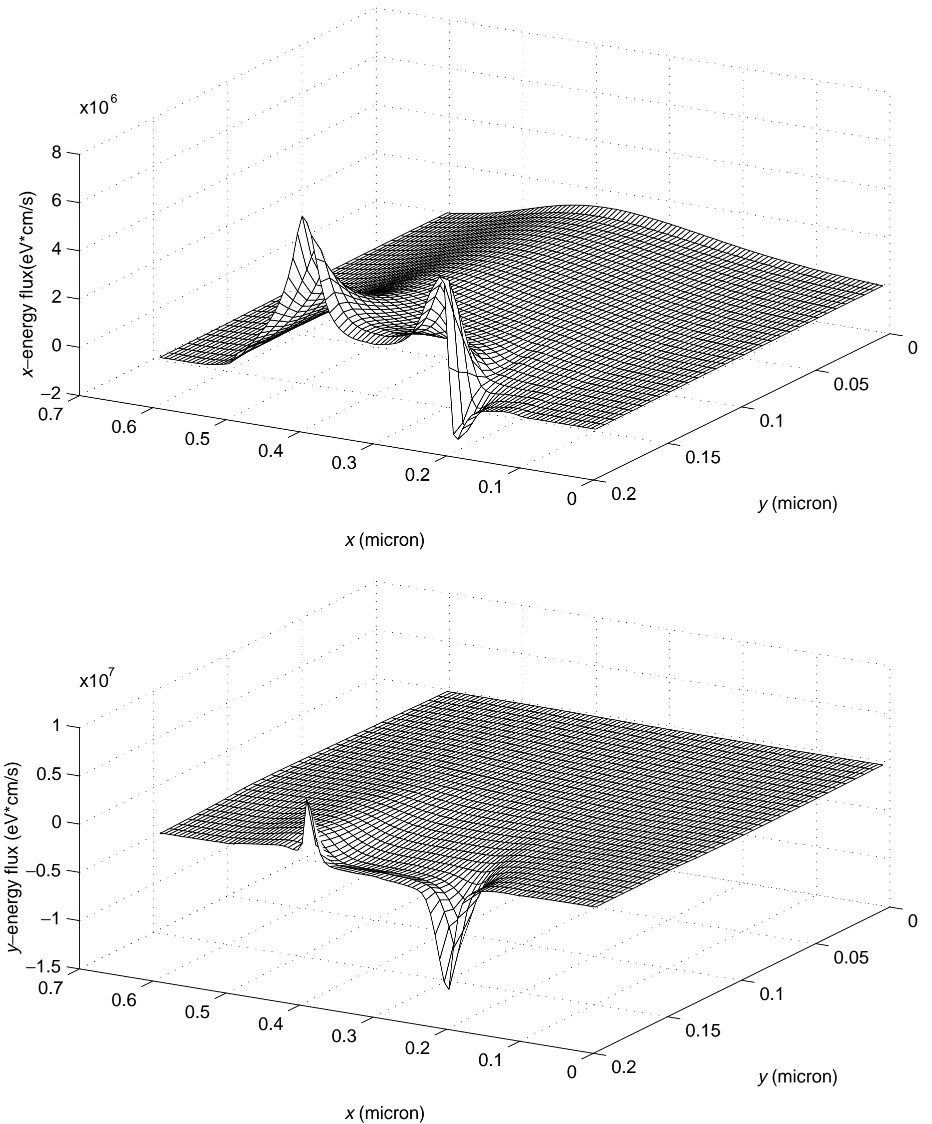

FIG. 7. Stationary solution (after 5 ps) for the energy-flux for $\Phi_b = 1$ V.

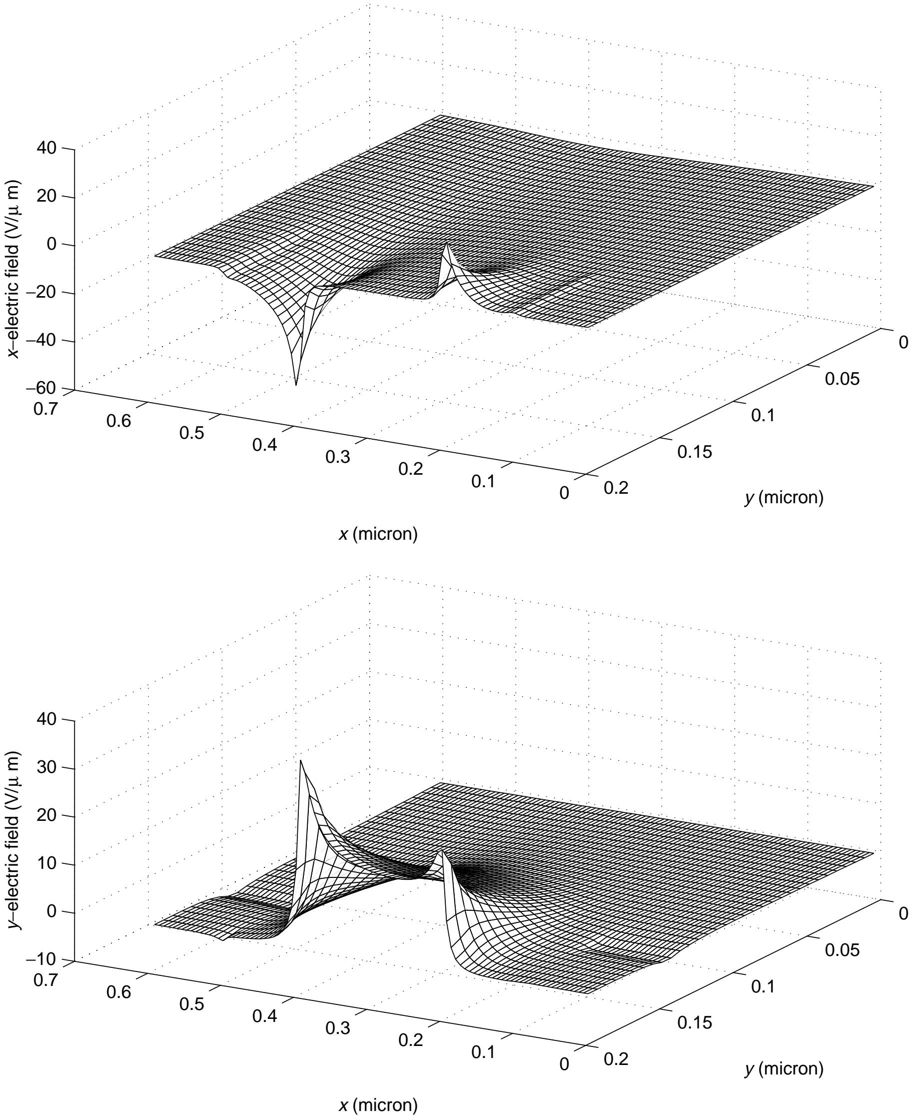

FIG. 8. Stationary solution (after 5 ps) for the x-component and y-component of the electric field for $\Phi_b = 1$ V.

powers between the semiconductor and the metal at homic contacts, the continuity of the energy flux leads to [35]

$$\kappa \mathbf{n} \cdot \nabla T = h(T_{ext} - T). \tag{39}$$

h is the thermal surface conductance, which characterizes the thermal contact between the semiconductor and the adjacent material that is at temperature T_{ext}. We assume $T_L = T_{ext}$ in our simulations.

In the special case of an ideal sink ($h \mapsto \infty$) $T = T_{ext}$ and consequently we have $\mathbf{q} = 0$. This implies in view of (38) the relations $(36)_4$ and $(37)_5$.

We start the simulation with the following initial conditions:

$$n(x, y, 0) = n_D(x, y) - n_A(x, y),\ W = W_0 = \frac{3}{2} k_B T_L,\ V^i = 0,\ S^i = 0, \quad i = 1, 2. \tag{40}$$

T_L is the room temperature of 300 K.

The main numerical problems in this work arise from the discontinuous doping and the boundary conditions at the Schottky barrier, which give rise there to sharp changes of several orders of magnitude in the density. The use of a *shock-capturing* scheme is almost mandatory for this problem.

In the first case we take $\Phi_b = 1$ V. The stationary solution is reached in a few picoseconds (less than 5). The code takes about 9 min and 10 s in a PC with a 1-GHz Pentium III microprocessor. After the inital restless behavior the solution becomes smooth and no signs of spurious oscillations are present. The numerical scheme seems suitably robust and is able to capture the main features of the solution. Only the Kane dispersion relation is considered here because the results obtained in the parabolic band approximation are rather unsatisfactory when high electric fields are involved, as shown in [7] for a silicon n^+–n–n^+ diode. The model has given good results when compared with Monte Carlo simulation in one-dimensional problems (see [9]). Unfortunately no Monte Carlo data are available to us for bidimensional cases and therefore we can compare the results only with those obtained by other hydrodynamical models.

The density is plotted in Fig. 4. As expected there is a depletion region beneath the gate. Moreover, one can see that the drain is less populated than the source.

Concerning the energy (Fig. 5) there are sudden variations near the gate edges. The mean energy of the electrons reaches a maximum value of about 0.35 eV in the part of the gate closest to the source.

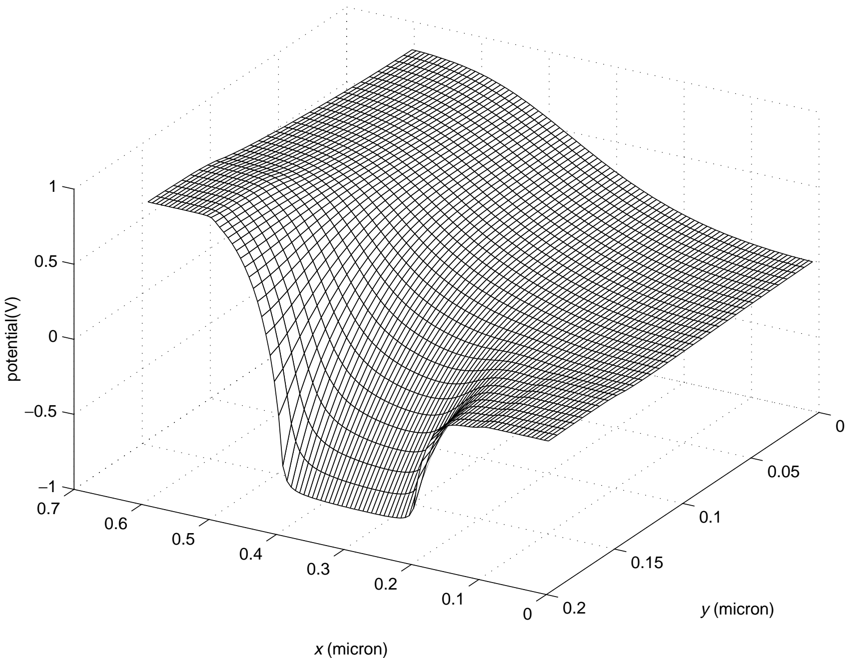

FIG. 9. Stationary solution (after 5 ps) for the electric potential for $\Phi_b = 1$ V.

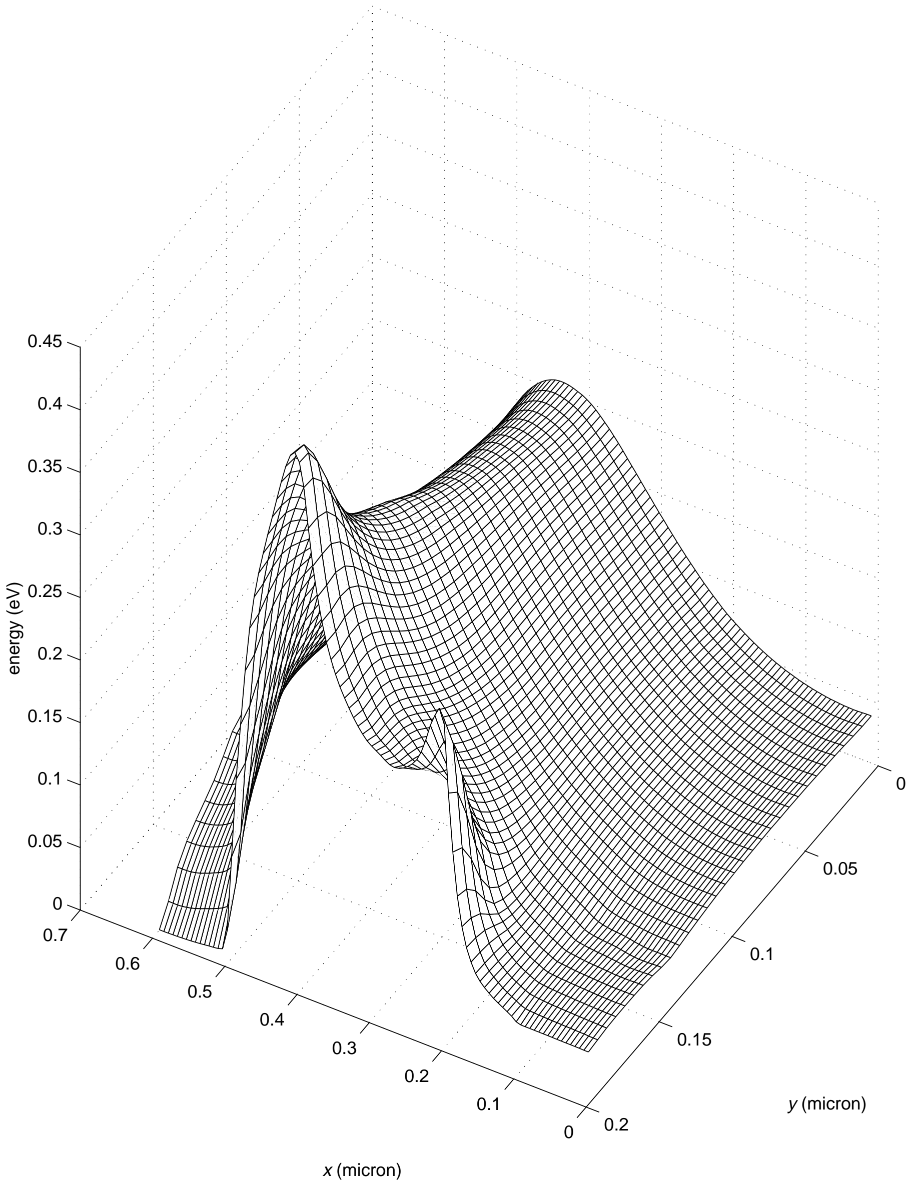

FIG. 10. Stationary solution (after 5 ps) for the energy density for $\Phi_b = 2$ V.

The results for the velocity are shown in Fig. 6. The higher values of the x-component are at the edges of the gate contact. This happens also for the y-component, but with a huge peak at the gate edge closest to the source. The behavior seems to indicate that there is a loss of regularity at the edge of the gate.

The shape of the energy flux (Fig. 7) is qualitatively similar to that of the velocity.

Very large tangential and normal components of the electric field (Fig. 8) are present again at the edges of the gate. For completeness the electric potential is also presented in Fig. 9.

The results are qualitatively similar to those presented in [32, 33] for all the variables except the y-component of the velocity, on account of the huge peak at the edge of the gate.

As a second test we take $\Phi_b = 2$ V. The code takes about 13 min and 30 s. The longer CPU time with respect to the previous simulation is due to the more restrictive CFL condition. There are not significant differences in the case of $\Phi_b = 1$ V for density and electric field. Concerning the other variables, the behavior of the solution is qualitatively similar to that in the case of $\Phi_b = 1$ V, but with higher values of the fields. The stationary solution for energy, velocity, and energy flux is shown in Figs. 10–12.

If we compare our results with those obtained in [33], where the standard model [20, 21] with relaxation times extracted from Monte Carlo data has been employed, one notes that qualitatively the numerical solutions are very similar. There is some quantitative difference in the peak of the energy, which is lower with our model, and the maximum values of the y-component of the velocity, which are lower in the model presented in [33].

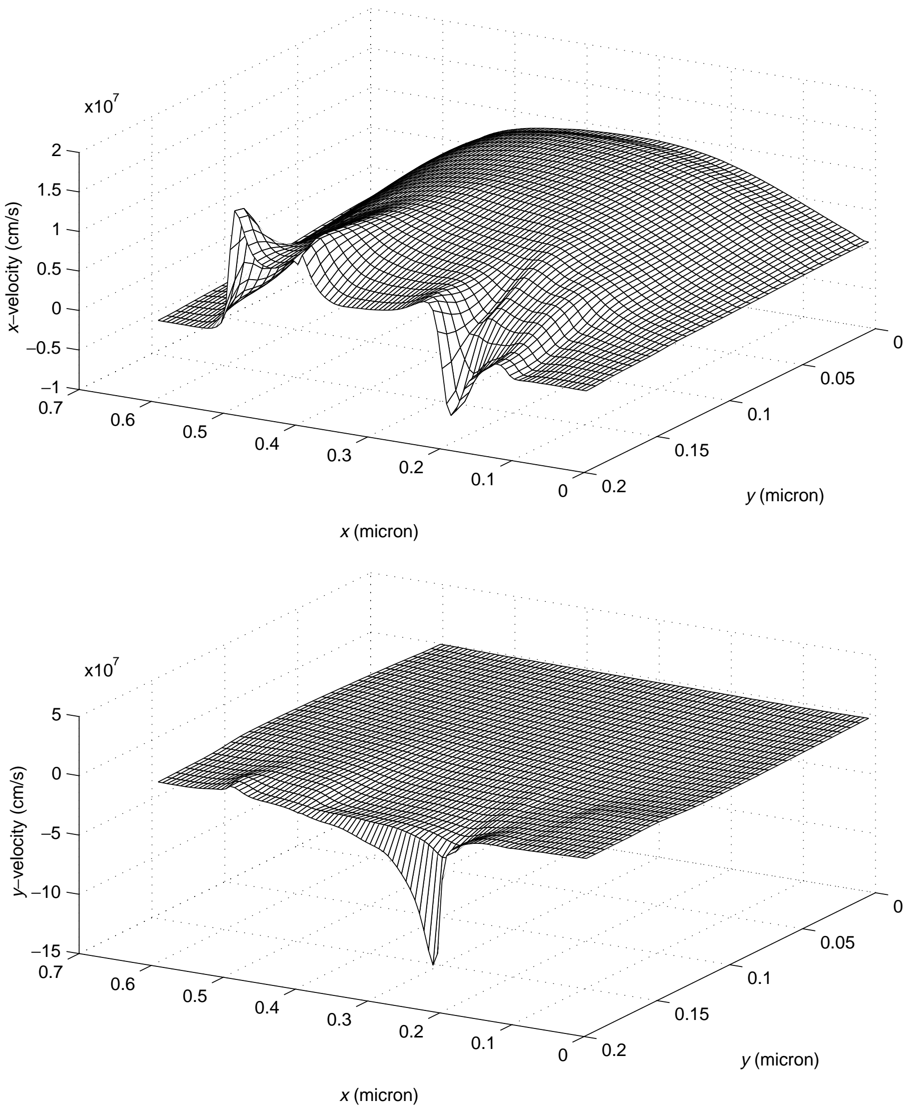

FIG. 11. Stationary solution (after 5 ps) for the x-component and y-component of the velocity for $\Phi_b = 2$ V.

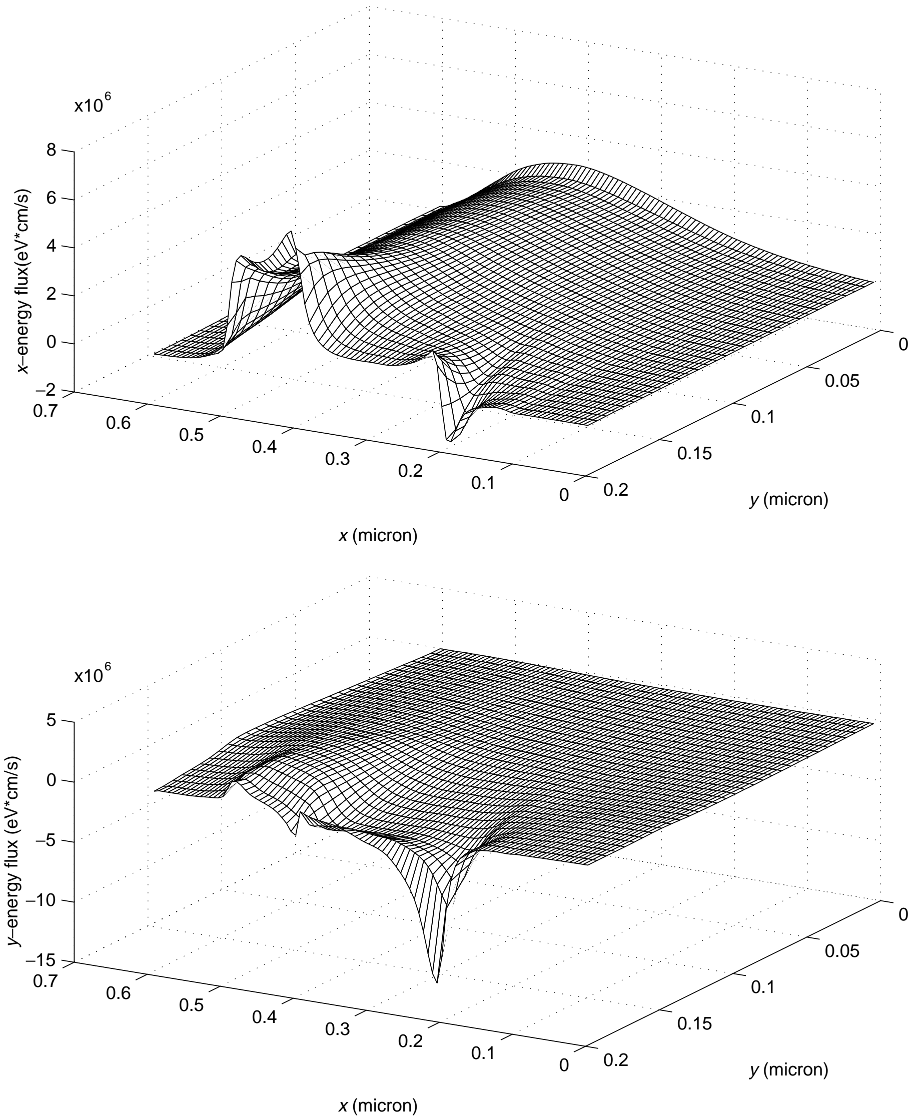

FIG. 12. Stationary solution (after 5 ps) for the energy flux for $\Phi_b = 2$ V.

APPENDIX: SUMMARY OF THE CLOSURE RELATIONS

In Table 1 we report the values of the physical parameters used in the simulations. Moreover, for the sake of completeness, we summarize up to first order in δ all the constitutive equations needed to close the balance equations (2)–(5). For more details see [1, 2].

Concerning the tensors U^{ij}, F^{ij}, and G^{ij}, one has

$$U^{ij} = U(W)\,\delta^{ij},\ F^{ij} = F(W)\,\delta^{ij},\ G^{ij} = G(W)\,\delta^{ij}, \tag{41}$$

with

$$U = \frac{2}{3\,d_0}\int_0^{\infty}[\mathcal{E}(1+\alpha\mathcal{E})]^{3/2}\exp\bigl(-\lambda^{W(0)}\mathcal{E}\bigr)\,d\mathcal{E}, \tag{42}$$

TABLE 1
Values of the Physical Parameters Used for Silicon

m_e	Electron rest mass	9.1095×10^{-28} g
m^*	Effective electron mass	$0.32\ m_e$
T_L	Lattice temperature	300 K
ρ	Density	2.33 g/cm^3
v_s	Longitudinal sound speed	9.18×10^5 cm/s
Ξ_d	Acoustic-phonon deformation potential	9 eV
α	Nonparabolicity factor	0.5 eV^{-1}
ϵ_r	Relative dielectric constant	11.7
ϵ_0	Vacuum dieletric constant	8.85×10^{-18} C/V μm

$$F = \frac{2}{3m^* d_0} \int_0^\infty \exp\left(-\lambda^{W(0)} \mathcal{E}\right) \frac{\mathcal{E}[\mathcal{E}(1+\alpha\mathcal{E})]^{3/2}}{1+2\alpha\mathcal{E}}\, d\mathcal{E}, \tag{43}$$

$$G = \frac{1}{nm^* d_0} \int_0^\infty \exp\left(-\lambda^{W(0)} \mathcal{E}\right) \left[1 + \frac{2(1+\alpha\mathcal{E})}{3(1+2\alpha\mathcal{E})^2}\right] \mathcal{E}^{3/2}\sqrt{1+\alpha\mathcal{E}}\, d\mathcal{E}. \tag{44}$$

$\lambda^{W(0)}(W)$ is the expression of the Lagrangian multipliers relative to the energy up to first order in δ (see [1]). It depends only on W and it is obtained by inverting the relation

$$W = \frac{\int_0^\infty \mathcal{E}\sqrt{\mathcal{E}(1+\alpha\mathcal{E})}(1+2\alpha\mathcal{E}) \exp\left(-\lambda^{W(0)}\mathcal{E}\right) d\mathcal{E}}{\int_0^\infty \sqrt{\mathcal{E}(1+\alpha\mathcal{E})}(1+2\alpha\mathcal{E}) \exp\left(-\lambda^{W(0)}\mathcal{E}\right) d\mathcal{E}}.$$

Note that U, F, and G depend only on W as a consequence of the fact that $\lambda^{W(0)}$ is a function of W alone.

The production terms are the sum of the term due to the elastic scatterings (acoustic phonon scattering) and of that due to inelastic phonon scatterings. Therefore the production matrix $C = (c_{ij})$ is given by the sum $C = C^{(ac)} + C^{(np)}$.

Concerning the acoustic phonon scattering, the contribution to the energy balance equation is zero while the production matrix $C^{(ac)} = (c_{ij}^{(ac)})$ can be written as $C^{(ac)} = A^{(ac)} B$. The coefficients b_{ij} of the matrix B are given by

$$b_{11} = \frac{a_{22}}{\Delta}, \quad b_{12} = -\frac{a_{12}}{\Delta}, \quad b_{22} = \frac{a_{11}}{\Delta}$$

with

$$a_{11} = -\frac{2p_0}{3m^* d_0}, \quad a_{12} = -\frac{2p_1}{3m^* d_0}, \quad a_{22} = -\frac{2p_2}{3m^* d_0}, \quad \Delta = a_{11}a_{22} - a_{12}^2,$$

$$d_k = \int_0^\infty \mathcal{E}^k \sqrt{\mathcal{E}(1+\alpha\mathcal{E})}(1+2\alpha\mathcal{E}) \exp\left(-\lambda^{W(0)}\mathcal{E}\right) d\mathcal{E}, \quad k = 0, 1, \ldots,$$

$$p_k = \int_0^\infty \frac{[\mathcal{E}(1+\alpha\mathcal{E})]^{3/2}\mathcal{E}^k}{1+2\alpha\mathcal{E}} \exp\left(-\lambda^{W(0)}\mathcal{E}\right) d\mathcal{E}, \quad k = 0, 1, \ldots.$$

The coefficients of the matrix $A^{(ac)}$ read

$$a_{11}^{(ac)} = \frac{\bar{K}_{ac}}{d_0} \int_0^\infty \mathcal{E}^2(1+\alpha\mathcal{E})^2(1+2\alpha\mathcal{E}) \exp\left(-\lambda^{W(0)}\mathcal{E}\right) d\mathcal{E}, \tag{45}$$

$$a_{12}^{(ac)} = \frac{\bar{K}_{ac}}{d_0} \int_0^\infty \mathcal{E}^3 (1+\alpha\mathcal{E})^2 (1+2\alpha\mathcal{E}) \exp\left(-\lambda^{W(0)}\mathcal{E}\right) d\mathcal{E}, \quad (46)$$

$$a_{21}^{(ac)} = \frac{\bar{K}_{ac}}{m^* d_0} \int_0^\infty \mathcal{E}^3 (1+\alpha\mathcal{E})^2 \exp\left(-\lambda^{W(0)}\mathcal{E}\right) d\mathcal{E}, \quad (47)$$

$$a_{22}^{(ac)} = \frac{\bar{K}_{ac}}{m^* d_0} \int_0^\infty \mathcal{E}^4 (1+\alpha\mathcal{E})^2 \exp\left(-\lambda^{W(0)}\mathcal{E}\right) d\mathcal{E}, \quad (48)$$

where

$$\bar{K}_{ac} = \frac{8\pi\sqrt{2}(m^*)^{3/2} K_{ac}}{3\hbar^3}, \qquad K_{ac} = \frac{k_B T_L \Xi_d^2}{4\pi^2 \hbar \rho v_s^2}.$$

Concerning the nonpolar phonon scattering the production term of the energy balance equation is given by $C_W = \sum_{A=1}^{6} C_{W_A}$, where for each valley

$$C_{W_A} = \frac{3}{2} \frac{\bar{K}_{np}}{d_0} \sum_{\pm} \left(n_B + \frac{1}{2} \mp \frac{1}{2}\right) \left[\exp\left(\pm \frac{\hbar\omega_{np}}{k_B T_L} \mp \lambda^{W(0)} \hbar\omega_{np}\right) - 1\right] \eta^{\pm}, \quad (49)$$

with

$$\eta^{\pm} = \int_{\hbar\omega_{np} H(1\mp 1)}^{\infty} \mathcal{E} \mathcal{N}_{\pm} \sqrt{\mathcal{E}(1+\alpha\mathcal{E})} (1+2\alpha\mathcal{E}) \exp\left(-\lambda^{W(0)\mathcal{E}}\right) d\mathcal{E}, \quad (50)$$

$$\mathcal{N}_{\pm} = \sqrt{(\mathcal{E} \pm \hbar\omega_{np})[1+\alpha(\mathcal{E} \pm \hbar\omega_{np})]} [1 + 2\alpha(\mathcal{E} \pm \hbar\omega_{np})], \quad (51)$$

and

$$\bar{K}_{np} = \frac{8\pi\sqrt{2}(m^*)^{3/2} K_{np}}{3\hbar^3}, \qquad K_{np} = Z_f \frac{(D_t K)^2}{8\pi^2 \rho \omega_{np}}.$$

H is the Heaviside function

$$H(x) = \begin{cases} 1 & \text{if } x > 0 \\ 0 & \text{otherwise.} \end{cases}$$

The coefficients of the production matrix $C^{(np)} = (c_{ij}^{(np)})$ are given by $c_{ij}^{(np)} = \sum_{A=1}^{6} c_{A_{ij}}^{(np)}$. For each valley one has $C^{(np)} = A^{(np)} B$, where the matrix $A^{(np)}$ has components

$$a_{11}^{(np)} = \frac{\bar{K}_{np}}{d_0} \sum_{\pm} \left(n_B + \frac{1}{2} \mp \frac{1}{2}\right) \int_{\hbar\omega_{np} H(1\mp 1)}^{\infty} \mathcal{N}_{\pm} \mathcal{E}^{3/2} (1+\alpha\mathcal{E})^{3/2} \exp\left(-\lambda^{W(0)}\mathcal{E}\right) d\mathcal{E}, \quad (52)$$

$$a_{12}^{(np)} = \frac{\bar{K}_{np}}{d_0} \sum_{\pm} \left(n_B + \frac{1}{2} \mp \frac{1}{2}\right) \int_{\hbar\omega_{np} H(1\mp 1)}^{\infty} \mathcal{N}_{\pm} \mathcal{E}^{5/2} (1+\alpha\mathcal{E})^{3/2} \exp\left(-\lambda^{W(0)}\mathcal{E}\right) d\mathcal{E}, \quad (53)$$

$$a_{21}^{(np)} = \frac{\bar{K}_{np}}{m^* d_0} \sum_{\pm} \left(n_B + \frac{1}{2} \mp \frac{1}{2}\right) \int_{\hbar\omega_{np} H(1\mp 1)}^{\infty} \mathcal{N}_{\pm} \frac{\mathcal{E}^{5/2} (1+\alpha\mathcal{E})^{3/2}}{1+2\alpha\mathcal{E}} \exp\left(-\lambda^{W(0)}\mathcal{E}\right) d\mathcal{E}, \quad (54)$$

$$a_{22}^{(np)} = \frac{\bar{K}_{np}}{m^* d_0} \sum_{\pm} \left(n_B + \frac{1}{2} \mp \frac{1}{2}\right) \int_{\hbar\omega_{np} H(1\mp 1)}^{\infty} \mathcal{N}_{\pm} \frac{\mathcal{E}^{7/2} (1+\alpha\mathcal{E})^{3/2}}{1+2\alpha\mathcal{E}} \exp\left(-\lambda^{W(0)}\mathcal{E}\right) d\mathcal{E}. \quad (55)$$

TABLE 2
Coupling Constants and Phonon Energies for Inelastic Scattering in Silicon

A	Z_f	$\hbar\omega$ (meV)	$D_t K$ (10^8 eV/cm)
1	1	12	0.5
2	1	18.5	0.8
3	4	19.0	0.3
4	4	47.4	2.0
5	1	61.2	11
6	4	59.0	2.0

The coupling constants and the values of the energy phonons for each valley are reported in Table 2 [34].

In order to speed up the computation, in the numerical code we do not evaluate U, F, G, τ_W, and the coefficients c_{ij} at each time step by using the above formulas. Instead we calculate in advance a numerical table of the variables as functions of the energy W and during the simulation we determine particular values by interpolation.

ACKNOWLEDGMENTS

This work has been partially supported by MURST, *ex fondi 60%*, and the project Problems of Kinetic Theory (1998), by the TMR program *Asymptotic Methods in Kinetic Theory*, Grant ERBFMRXCT970157, and by CNR Grant 97.04709.PS01.

REFERENCES

1. A. M. Anile and V. Romano, Non parabolic band transport in semiconductors: closure of the moment equations, *Continuum Mech. Thermodyn.* **11**, 307 (1999).
2. V. Romano, Non parabolic band transport in semiconductors: closure of the production terms in the moment equations, *Continuum Mech. Thermodyn.* **12**, 31 (2000).
3. H. Nessyahu and E. Tadmor, Non-oscillatory central differencing for hyperbolic conservation law, *J. Comp. Phys.* **87**, 408 (1990).
4. G.-S. Jiang and E. Tadmor, Nonoscillatory central schemes for multidimensional hyperbolic conservation laws, *SIAM J. Sci. Comput.* **19**, 1892 (1998).
5. F. Liotta, V. Romano, and G. Russo, Central schemes for systems of balance laws, *Int. Ser. Numer. Math.* **130**, 651 (1999).
6. F. Liotta, V. Romano, and G. Russo, Central schemes for balance laws of relaxation type, *SIAM J. Numer. Anal.* **38**, 1337 (2000).
7. V. Romano, Nonparabolic band hydrodynamical model of silicon semiconductors and simulation of electron devices, *Math. Methods Appl. Sci.* **24**, 439 (2001).
8. A. M. Anile, O. Muscato, and V. Romano, Moment equations with maximum entropy closure for carrier transport in semiconductors devices: validation in bulk silicon, *VLSI Design* **10**, 335 (2000).
9. O. Muscato and V. Romano, *Simulation of Submicron Silicon Diode with a Non-Parabolic Hydrodynamical Model Based on the Maximum Entropy Principle*, IWCE-7, Glasgow 2000, preprint archive TMR project Asymptotic Methods in Kinetic Theory, available at http://www.math.tu-berlin.de/~tmr.
10. S. Selberherr, *Analysis and Simulation of Semiconductor Devices* (Springer-Verlag, Vienna/New York, 1984).
11. W. Hänsch, *The Drift-Diffusion Equation and Its Applications in MOSFET Modeling* (Springer-Verlag, Vienna, 1991).

12. P. Markowich, C. A. Ringhofer, and C. Schmeiser, *Semiconductor Equations* (Springer-Verlag, Vienna, 1990).
13. D. Chen, E. C. Kan, U. Ravaioli, C.-W. Shu, and R. Dutton, An improved energy-transport model including nonparabolicity and non-maxwellian distribution effects, *IEEE Trans. Electron Device Lett.* **13**, 26 (1992).
14. E. Lyumkis, B. Polsky, A. Shir, and P. Visocky, Transient semiconductor device simulation including energy balance equation, *Compel* **11**, 311 (1992).
15. N. B. Abdallah and P. Degond, On a hierarchy of macroscopic models for semiconductors, *J. Math. Phys.* **37**, 3308 (1996).
16. I. Müller and T. Ruggeri, *Rational Extended Thermodynamics* (Springer-Verlag, Berlin, 1998).
17. D. Jou, J. Casas-Vazquez, and G. Lebon, *Extended Irreversible Thermodynamics* (Springer-Verlag, Berlin, 1993).
18. C. D. Levermore, Moment closure hierarchies for kinetic theories, *J. Stat. Phys*. **83**, 331 (1996).
19. A. M. Anile and O. Muscato, Improved hydrodynamical model for carrier transport in semiconductors, *Phys. Rev. B* **51**, 16728 (1995).
20. K. Blotekjaer, Transport equations for electron in two-valley semiconductors, *IEEE Trans. Electron Devices* **ED-17**, 38 (1970).
21. G. Baccarani and M. R. Wordeman, An investigation on steady-state velocity overshoot in silicon, *Solid-State Electron.* **29**, 970 (1982).
22. V. Romano and G. Russo, Numerical solutions for hydrodynamical models of semiconductors, *Math. Models Methods Appl. Sci.* **10**, 1099 (2000).
23. A. M. Anile, V. Romano, and G. Russo, Extended hydrodynamical model of carrier transport in semiconductors, *SIAM J. Appl. Math.* **61**, 74 (2000).
24. A. Gnudi, D. Ventura, and G. Baccarani, Modeling impact ionization in BJT by means of spherical harmonics expansions of the Boltzmann transport equation, *IEEE Trans. Comput. Aided Design* **12**, 1706 (1993).
25. M. C. Vecchi and M. Rudan, Modeling electron and hole transport with full-band structure effects by means of the spherical-harmonics expansion of the BTE, *IEEE Trans. Electron Devices* **45**, 230 (1998).
26. T.-W. Tang, S. Ramaswamy, and J. Nam, An improved hydrodynamical transport model for silicon, *IEEE Trans. Electron Devices* **40**, 1469 (1993).
27. N. W. Ashcroft and N. D. Mermin, *Solid State Physics* (Sounders College, Philadelphia, 1976), Int. Ed.
28. E. F. Toro, *Riemann Solvers and Numerical Methods for Fluid Dynamics* (Springer-Verlag, Berlin, 1997).
29. R. J. LeVeque, *Numerical Methods for Conservation Laws* (Birkhäuser, Zürich, 1992).
30. A. Harten and S. Osher, Uniformily high-order accurate nonoscillatory scheme I, *SIAM J. Numer. Anal.* **24**, 279 (1987).
31. J. W. Jerome and C.-W. Shu, Energy models for one-carrier transport in semiconductor devices, in *Semiconductors Part II, The IMA Volumes in Mathematics and Its Applications*, edited by N. M. Coughran, J. Cole, P. Lloyd, and J. K. White (Springer-Verlag, New York, 1994), pp. 185–207.
32. W.-K. Yip, M. Shen, and M.-C. Cheng, *Hydrodynamic Modeling of Short-Channel Devices Using an Upwind Flux Vector Splitting Scheme*, preprint (2000).
33. M. Shen, M.-C. Cheng, and J. J. Liou, *A Generalized Finite Element Method for Hydrodynamic Modeling of Short-Channel Devices*, preprint (2000).
34. C. Jacoboni and L. Reggiani, The Monte Carlo method for the solution of charge transport in semiconductors with application to covalent materials, *Rev. Mod. Phys.* **55**, 645 (1983).
35. G. Wachutka, Rigorous thermodynamic treatment of heat generation and conduction in semiconductor device modeling, *IEEE Trans. Comput. Aided Design* **9**, 1141 (1990).